RSC Advances

ROYAL SOCIETY OF CHEMISTRY

www.rsc.org/advances

Ultra-large-scale Production of Ultrasmall Superparamagnetic Iron Oxide Nanoparticles for T_1-weighted MRI

Yuan-Peng Rui,[ζ, ‡] *Bo Liang,*[ζΔ, ‡] *Fenglin Hu,*[Φ, ‡] *Jie Xu,*[ζ] *Yi-Feng Peng,*[ζ] *Pei-Hao Yin,*[ζ,*] *Yourong Duan,*[Φ,ς,*] *Chunfu Zhang,*[Φ,Ψ,*] *Hongchen Gu*[Φ]

[ζ] Department of Radiology, Putuo Hospital, Shanghai University of Traditional Chinese Medicine, Shanghai 200062, China

Δ Department of Oncology, Tongde Hospital of Zhejiang Province, Hangzhou, 310012, Zhejiang Province, China

[Φ] State Key Laboratory of Oncogenes and Related Genes，Shanghai Cancer Institute, School of Biomedical Engineering，Shanghai Jiao Tong University, Shanghai 200030, China.

[ς] State Key Laboratory of Oncogenes and Related Genes, Shanghai Cancer Institute, Renji Hospital, School of Medicine, Shanghai Jiao Tong University

[Ψ] Department of Nuclear Medicine, Rui Jin Hospital, School of Medicine, Shanghai Jiao Tong University, Shanghai, 200025, P. R. China

* Corresponding authors

[‡] These authors contributed equally

Electronic supplementary information (ESI) available: the detailed procedure for calculation of free carboxylic groups on an USPIO, photograph of PAA@USPIOs in large-scale production,

TGA curves and auto acid-base titration curve of PAA@USPIOs, dose optimization of PAA@USPIOs for MRA and hematology analysis of mice are provided

Keywords: PAA@USPIOs; T_1 contrast agent; MRI; iron oxide

Abstract Ultrasmall superparamagetic iron oxide (USPIO) nanoparticles with high stability in physiological conditions have great potentials for T_1-weighted MRI. In current study, we developed a procedure for ultra-large-scale production of USPIOs (1.5 kg per batch) for T_1-weighted MRI. The USPIOs were coated with poly(acrylic acid) (PAA@USPIOs), uniform in size (~ 4.5 nm) and very stable in physiological conditions even after sterilized by autoclave. Due to its small size, PAA@USPIOs demonstrated good T_1 MRI contrast effect and could be used for both first-pass and steady-state magnetic resonance angiography (MRA). After injected with PAA@USPIOs at the dose of 135 μmol Fe/kg, the head-neck vasculatures and abdominal artery of rabbits and the coronary artery of pigs could be clearly visualized by T_1-weighted MRI. Moreover, PAA@USPIOs was highly tolerable by animals. Our study indicated that the procedure developed in this study has a great promise for large-scale production of USPIOs for T_1-weighted MRI for future clinical applications.

1. Introduction

Due to their high susceptibility, superparamagnetic iron oxide (SPIO) nanoparticles are conventionally used as T_2 MRI contrast agents (negative contrast). [1-4] However, when the size of the particles is reduced, the susceptibility, thus their T_2 effect, is reduced accordingly. [5-7] On the contrary, the particle surface area to volume ratio, thus the number of iron ions exposed on the particle surface, increases dramatically. Iron ions (Fe^{2+} and Fe^{3+}) could induce the local relaxation change of the nearby water protons and mainly reduce T_1, providing positive contrast on T_1-weighted MR images. [8] Small-sized SPIOs demonstrate good T_1 contrast effect and have been explored for magnetic resonance angiography (MRA). [9-12] However, if the particles should act as T_1 contrast agent, a size limitation for the superparamagnetic core is around 5 nm and aggregation of the particles has to be completely prevented. [13]

SPIOs can be conveniently prepared by co-precipitation of ferric and ferrous ions under the alkaline conditions in the presence of coating materials, such as PEG, dextran and its derivatives. [14, 15] Co-precipitation procedure can be easily scaled up. Currently, clinically approved SPIOs (i.e. Feridex, Resovist and Ferumoxytol) are produced by this way [3, 16] However, co-precipitation method usually leads to poor crystallinity and broad size distribution (4 ~ 20 nm). [7, 17] Small-sized SPIOs are acquired by size screening, which is costly and low productive. [18] Alternatively, thermal decomposition of an appropriate iron precursor (e. g. iron oleate, iron acetylacetonate and dicyclopentadienyl iron) in high boiling nonpolar solvents has been demonstrated to be an effective method to produce SPIOs with great monodispersity, high crystallinity and tunable sizes, [19-22] and this procedure can also be scaled up. [23] However, SPIOs produced by this way are poorly dispersed in aqueous solution due to their hydrophobic surface

coatings and have to be transferred into being hydrophilic for biomedical uses, which precludes production in large scale for clinical applications. [24, 25]

Thermal decomposition of iron precursors in polar solvents has been explored to produce hydrophilic SPIOs with well-defined size. [7, 26, 27] Polyols, such as ethylene glycol (EG), di(ethylene glycol) (DEG), triethylene glycol (TREG), are among such solvents and have been used as media to prepare iron oxide nanoparticles with various sizes. [28-30] For instances, water-dispersible iron oxide nanoparticles with a size range of 3~11 nm in DEG solvent has been reported. [29] However, the colloidal stability of the nanoparticles at the physiological conditions is poor, which makes them far from optimal for biomedical applications. To improve the colloidal stability, in-suit or post treatments of the particles with coating materials have been developed. [1, 31-33] Despite recent synthetic progress, it remains a challenge to prepare monodisperse USPIOs with good colloidal stability under physiological conditions for T_1-weighted MRI in large scale.

In this study, we developed a novel method for ultra-large-scale preparation of poly(acrylic acid)-coated USPIOs (PAA@USPIOs) with size around 4.5 nm in one pot. As-prepared USPIOs are very stable in physiological conditions, and demonstrate good T_1 effect both in vitro and in vivo.

2. Materials and Methods

Materials Di(ethylene glycol) (DEG, $(HOCH_2CH_3)_2O$, 99%) was purchased from Sigma-Aldrich (St. Louis, MO). Poly(acrylic acid) (PAA, 50 wt%, solution in water, MW5000) was purchased from Acros. Other chemicals were obtained from Sinopharm Chemical Reagent Co. Ltd. (Shanghai, China) if not indicated otherwise. Ultrafiltration membranes (NMWL=300,000)

and membrane filters with pore sizes of 0.22 μm and 0.1 μm were purchased from Millipore (Shanghai, China).

Small-scale synthesis of PAA-coated USPIOs (PAA@USPIOs) PAA@USPIOs were synthesized by polyol method assisted by microwave heating. In brief, PAA (8 mmol) and $FeCl_3$ (4 mmol) were dissolved in DEG (30 mL). Nine milliliter of the mixture was transferred into a 50 mL round flask and heated by microwave (Discover S-Class, CEM) under vigorous stirring. When the temperature reached 220 ^{o}C, 2 mL NaOH solution (in DEG, 100 mg/mL, 80 ^{o}C) was rapidly injected. The resulting mixture was further heated for 10 min and then cooled down to the ambient temperature. As-prepared nanoparticles were precipitated with a mixture of ethanol and ethyl acetate (1:3, v/v), washed with ethanol three times and then dispersed into water. Next, the suspension was purified with a millipore ultrafiltration device (NMWL=300,000). After purification, the particles were spray-dried, dispersed in phosphate buffer solution (PBS, pH=7.4) and sterilized by autoclave.

Large-scale production of PAA@USPIOs For large-scale production of PAA@USPIOs, a microwave device with 30 kilowatt power and 50 liter volume was customized. The volumes of the PAA and $FeCl_3$ mixture and sodium hydroxide solution were 32.8 L and 7.2 L, respectively. The concentrations of the reactants and the procedures for the preparation and purification were same as those described above.

Characterizations The size, morphology and crystal structure of the particles were evaluated using transmission electron microscopy (TEM, JEOL 2010). Samples for TEM and high resolution TEM analysis were prepared by spreading a drop of the dilute nanoparticle dispersion

on the amorphous carbon-coated copper grids and then drying them in air. The average particle size was determined by measuring the diameters of more than 150 particles in the TEM images.

To further determine the crystal structure of the particles, X-ray diffraction (XRD) was performed on a Rigaku D/max-2400 type auto X-ray diffract meter (Rigaku, Japan) at 40 kV with Cu/Kα radiation (λ = 0.1542 nm). A slow scanning step of 0.31^{o}/min between 32^{o} and 46^{o} was performed to determine the particle size with Debye-Scherrer formula.

The hydrodynamic sizes and the zeta potentials (at pH = 7.4) were measured using a Malvern Instruments Zetasizer Nano Series Nano-ZS. The mass fraction of PAA coating was determined by a thermogravimetric analyzer (TGA, Mettler Toledo TGA/DSC 1/1600). The samples were lyophilized and heated from 30 ^{o}C to 1000 ^{o}C at 10 ^{o}C /min under a nitrogen flow.

To verify PAA coating, Fourier transform infrared (FTIR) measurements were performed by an EQUINOX 55 FTIR instrument (Bruker, Germany). For this purpose, all samples were ground and mixed with KBr and then pressed to form pellets. Spectra were recorded in the wave number interval between 4000 and 400 cm^{-1}. The background spectrum was subtracted from the sample spectrum. Each spectrum was acquired three times, and an average of the three measurements was taken and analyzed.

The free carboxylic groups on the particle surface were determined by titration with sodium hydroxide using a potential-conductivity titrator (Mettler Toledo, T50). For this purpose, PAA@USPIOs (8.72 mg/mL, 0.4 mL) were dispersed into 50 mL water, into which hydrochloric acid (0.01M, 5 mL) was added to protonate free carboxylate groups on PAA. Titration was performed with 0.1 M sodium hydroxide solution.

The magnetic properties of the particles were investigated by using a vibrating sample magnetometer (VSM, LakeShore7300, CA). The magnetization (M, emu g^{-1}) of the samples was measured as a function of the magnetic field (H, Oe) at 300 K. The longitudinal (T_1) and transverse (T_2) relaxation times were measured on a Bruker mq60 nuclear magnetic resonance analyzer (60 MHz, 1.41T) at 37 ^{o}C. An inversion recovery (IR) pulse sequence and a Carr-Purcell-Meiboom-Gill (CPMG) spin echo sequence were used in T_1 and T_2 measurements. The iron concentrations were determined using inductively coupled plasma optical emission spectrometry (ICP-OES, ICAP-6300, Thermo Fisher, Portsmouth, New Hampshire). The $T_{1,2}$ relaxivities ($r_{1,2}$) were deduced by fitting inverse relaxation times ($1/T_{1,2}$) as a function of the iron concentrations.

Phantom study To demonstrate T_1 effect of the particles *in vitro*, PAA@USPIOs were dispersed in water with different concentrations (0.01, 0.05, 0.1, 0.2, 0.5 mM) and placed in a water tank. [34] MRI was performed with a 1.5 T MRI scanner (Signa Excite 1.5T Twinspeed) using a clinical head coil with T_1 (TR = 500ms, TE = 30 ms, Matrix = 265 × 265 mm, slice thickness = 5 mm, NEX = 3) and T_2 (TR = 2000ms, TE = 102 ms, Matrix = 265 × 265 mm, Slice thickness = 5 mm, NEX = 3) weighted spin echo sequence.

Cytotoxicity of PAA@USPIOs The cytotoxicity of PAA@USPIOs was determined quantitatively by 3-(4, 5-dimethylthiazol-2-yl)-2, 5-diphenyltetrazolium bromide (MTT) reduction method using fibroblast L929 cells. For this purpose, the cells (5×10^3) were seeded in each well of 96 well plate and incubated with the PAA@USPIOs at different concentrations (20, 40, 80, 160, 320 and 640 μg/mL in iron) for 24, 48 and 72 h. After incubation, the medium were removed and the cells were washed with PBS. Subsequently, 100 μL of DMEM (without serum)

with 0.5 mg/mL of MTT reagent was added to each well and incubated for 4 h at 37 °C. After incubation, the culture media containing unreacted MTT was carefully removed from each well and the remaining blue formazan crystals formed in living cells were solubilized with 150 μL DMSO. The absorbance at 490 nm was measured using a Wallace 1420 multilabel counter VICTOR3 (PerkinElmer, Baltimore, MD). Cell viability was expressed as a percentage of the absorbance of cells incubated with PAA@USPIOs to that of cells maintained in normal culture medium.

Magnetic resonance angiography (MRA) To evaluate T_1 contrast effect of PAA@USPIOs in vivo, MRA of rabbits was first performed. Animal experiments were approved by the animal care and use committee of Shanghai Jiao Tong University. MRI was performed on a 1.5 T GE Medical Systems (Signa Excite 1.5T Twinspeed) using a surface coil with 4 independent receiver channels. Rabbits were anaesthetized with pentobarbital sodium at the dose of 45 mg/kg through ear vein injection.

To explore the optimal dose for MRA, T_1-weighted MRI at coronal and sagittal orientations were acquired using the 3D fast low angle shot (TOF-FSPGR) sequence (TR = 1.6 ms, TE = 6.1 ms, Filp Angle = 40 ^{o}, FOV = 28 cm, Matrix = 256 × 160, Band width = 31.2 kHz, Slice thickness = 0.8 mm). The rabbits were injected intravenously through ear vein with different doses of PAA@USPIOs (20、40、70、85、100、135、200 μmol Fe/kg) with three rabbits for each dosage. Acquisitions were done at first pass, 3 and 30 minutes post contrast medium administration. The abdominal aorta was imaged. In addition, MRA of head-neck vasculatures was also performed at the dose of 135 μmol Fe/kg.

To demonstrate the potential of PAA@USPIOs for first-pass MRA, a comparison study in first-pass MRA with clinically well-established gadolinium contrast agent Magnevist (Schering, Berlin, Germany) was conducted. For this purpose, three rabbits were injected intravenously with PAA@USPIOs at the dose of 135 μmol Fe /kg b. w. or Magnevist at the dose of 200 μmol Gd /kg b. w. MRI was performed immediately after injection and the imaging procedures were same as that described above. Signal intensities (SI) were analyzed by standard region-of-interest (ROI) measurements using ROI values placed in the lumen of aorta (SI_{aorta}) and outside the body (SI_{noise}). Signal to noise ratio (SNR) was calculated by dividing SI_{aorta} to SI_{noise}.

A comparison of PAA@USPIOs to SHU555C (Schering AG, Berlin, Germany) for first-pass and steady-state MRA was also performed. For this purpose, three rabbits were injected with SHU555C or PAA@USPIOs at the dose of 135 μmol Fe/kg b. w. and MR imaging procedures were same as that described above.

Coronary MRA in pigs To further demonstrate the T_1 effect of PAA@USPIOs *in vivo* and the potential of the particles for coronary artery imaging, coronary MRA of pigs was performed. Pigs (~ 30 kg) were anaesthetized with pentobarbital sodium at the dose of 45 mg/kg and administered intravenously with the particles at the dose of 135 μmol Fe/kg b. w. MRI was performed on a 3 T GE MRI scanner (Signa HDxt, 3T) using a Small AA only 30 coil and a 3D VascTOF FSPGR sequence. The sequence parameters were FOV 32 cm, Frequency 320, Phase 320, NEX 3, BW 62.5 kHz, RES Gating setting: Trigger point 10%/Trigger window 20%, Cardic Gating setting: automatic. Images were acquired before contrast administration and at 15 and 180 minutes post-contrast. Contrast between coronary artery and myocardium ($SNR_{myocardium}$) was calculated using the SI values of blood in the right coronary artery and of the adjacent myocardium.

Acute single dose toxicity in mice To evaluate the acute toxicity of PAA@USPIOs, an approximate LD_{50} was determined by a called 'staircase method'. Mice (Kunming mouse, ~ 30 g, Slaccs, Shanghai, China) were injected with PAA@USPIOs at five dose levels ranging from 0.25 to 4 mmol Fe/kg (0.25, 1, 2, 3 and 4 mmol Fe/kg) with ten mice in each dose group. After injection of the first dose group, physical status and death of the mice were observed. Fifteen minutes later, if the mice were dead, the dose for the next group was decreased. Otherwise, the dose was increased. LD_{50} was calculated according to the modified Spearman-Karber method. [35]

Repeated dose toxicity in mice To evaluate the long term toxicity, mice were injected with PAA@USPIOs at different doses (0.73, 1.46 and 2.92 mmol Fe/kg) with 6 mice (3 males and 3 females) in each dose group. Another six healthy mice were injected with PBS used as a control group. PAA@USPIOs were injected into the tail vein every other day until the intended dose was achieved, which last 14 days. [36, 37] Two days after the end of the treatment period, the mice were sacrificed and the major organs (heart, spleen, liver, lung, and kidney) were harvested for histological studies. For this purpose, the organs were fixed in 4% formalin, imbedded in paraffin and then processed for hematoxylin and eosin (H&E) (Aladdin, Ontario, CA, USA) staining according to the protocol provided by the manufacturer. In detail, representative 5μm tissue cross-sections were cut. After being mounted on glass slides, the sections were dewaxed in xylene, dehydrated in ethanol, and then washed briefly in deionized water. Subsequently, the sections were stained with hematoxylin solution for 8 minutes, washed in running tap water for 5 minutes, differentiated in 1% acid alcohol for 30 seconds, and then returned to blue with ammonia solution (0.2%, v/v). After washing in running tap water for 5 min and rinsing in alcohol (95%), the tissue slices were counterstained with eosin for 2 min and then examined under a digital microscope (Leica DM2500, Houston, Texas). Moreover, the blood samples were

also collected for blood routine examination and blood chemistry analysis. Blood routine examination included red blood cells (RBC), white blood cells (WBC), mean corpuscular hemoglobin (MCH), mean corpuscular volume (MCV), mean corpuscular hemoglobin concentration (MCHC), hemoglobin (HGB), percentage of lymphocyte in white blood cells (LY), percentage of neutrophile granulocyte in white blood cells (NE) and platelet count (PLT). Blood chemistry analysis included liver function markers (alkaline phosphatase (ALP), alanine aminotransferase (ALT), aspartate aminotransferase (AST)), serum albumin (ALB), kidney function markers (urea nitrogen (BUN) and creatinine (CRE)). All the blood parameters were measured in Shanghai Putuo Hospital.

Statistical analyses All data presented are the average ± SD of experiments repeated three or more times. Where appropriate, a Student's t-test was used to determine if differences were statistically significant. A P value of < 0.05 was considered to indicate significant differences between groups.

3. Results and Discussion

Synthesis and characterizations of PAA@USPIOs PAA@USPIOs were synthesized by a polyol process using di(ethylene glycol) (DEG) as a solvent assisted by microwave heating. For small-scale synthesis, sodium hydroxide solution (1.6 mL, 2.5 M in DEG) was quickly injected into a pre-heated mixture (9 mL) of ferric chloride solution (0.13 M) and poly(acrylic acid) (MW 5000, 0.27 M) under magnetic stirring and the reaction was carried out at 220 ^{o}C for 10 min. For ultra-large-scale production, a microwave device with 30 kilowatt power and 50 liter volume was customized for heating. The concentrations of the reactants were same as those for small-scale

synthesis, but the volumes were enlarged, 32.8 liters for the mixture of ferric chloride and poly acrylic acid and 7.2 liters for sodium hydroxide. Following the same procedure, one batch of about 1.5 kg nanoparticles (dry power) could be produced (Figure S1). Figure 1A shows the representative TEM images of the as-prepared nanoparticles. It is found that the particles are uniform and 4.5 ± 0.5 nm in size (Figure 1B). High resolution TEM analysis (Figure 1A, insert) indicates that the particle is a well-ordered single-domain crystal. Distance between two adjacent lattice fringes is 0.253 nm, corresponding to the lattice spacing of (311) planes of a face-centered cubic lattice of Fe_3O_4. [38, 39]

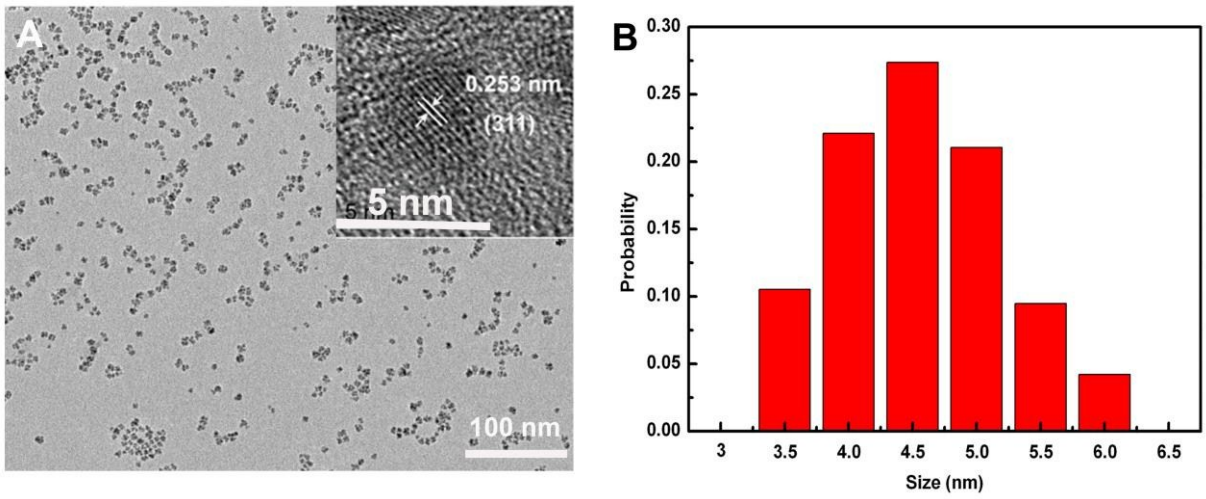

Figure 1 A, B TEM images of PAA@USPIOs (A, insert: high resolution TEM of the particles) and its size distribution (B). PAA@USPIOs are uniform and about 4.5 nm in size.

DEG in this study serves not only as a high boiling polar solvent but also a reducing agent, which partially reduces trivalent ion (in the form of $Fe(OH)_3$ under the high alkaline condition) into divalent ion ($Fe(OH)_2$). $Fe(OH)_3$ and $Fe(OH)_2$ are subsequently dehydrated at high temperature to form iron oxide nanoparticles. [29, 40] Therefore, different from the conventional

co-precipitation and thermal decomposition methods, inert gas protection is unnecessary; this is beneficial for large-scale production.

Microwave-assisted synthesis is a rapid, energy-efficient, and environmentally friendly approach for nanomaterial preparation, by which different types of nano materials have been synthesized. [41, 42] Compared to the conventional heating in a furnace, microwave provides fast and uniform heating of the solvents, so that homogeneous nucleation and crystal growth can be achieved within a much shortened period. [43] Uniform and fast heating contributes to mono-disperse, small-sized nanostructures obtained in this study.

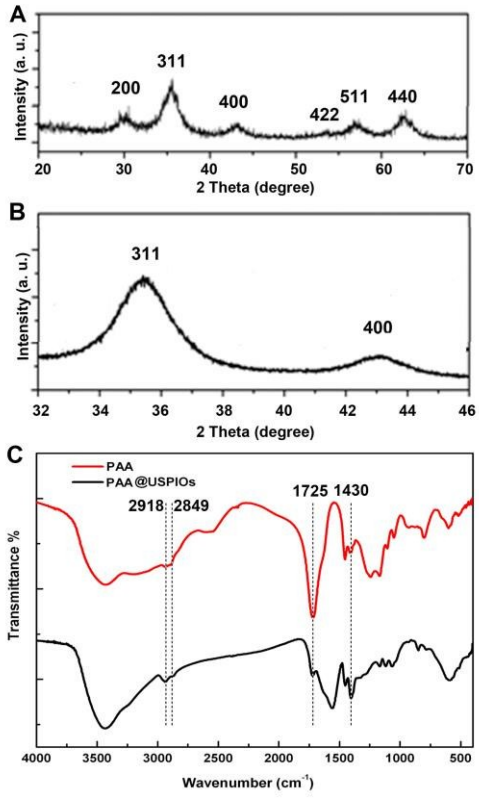

Figure 2 A, XRD pattern of PAA@USPIOs. B, XRD pattern of PAA@USPIOs between 32° and 46° with a low scanning step. C, FTIR spectra of PAA and PAA@USPIOs.

The crystalline structures and phase composition of PAA@USPIOs were further determined by X-ray diffraction (XRD). XRD pattern shows peaks at 30.11, 35.41, 43.11, 53.41, 57.11 and 62.61 degree (Figure 2A), which can be indexed to (220), (311), (400), (422), (511) and (440) lattice planes of the spinel structure (JCPDS card no. 01-082-1533) known for magnetite crystal.[6] No other peaks are detected, indicating that the product is pure phase Fe_3O_4. [39]

To verify the particle size observed by TEM, particle size was also calculated by the Debye-Scherrer's formula. For this purpose, XRD was performed with low scanning speed. Figure 2B shows the diffraction pattern between 32 ^{o} and 46 ^{o} at a scanning step of 0.31^{o}/min. The particle size calculated from (311) and (400) peaks is 4.8 nm, being consistent with the TEM statistical average size (4.5 ± 0.5 nm).

To explore the surface properties of the nanoparticles, Fourier transform infrared (FTIR) spectrum, thermal gravity analysis (TGA) and zeta-potential measurement were performed. The FTIR spectra of both PAA and PAA@USPIOs (Figure 2C) show absorption bands at 2849 and 2918 cm^{-1}, which arise from symmetric and asymmetric C-H stretch bands of methyl and methylene groups in PAA, respectively. [44] Bands at 1725 cm^{-1} is characteristic of C=O stretching mode of carboxylic groups, which is strong for PAA and become weak after USPIO coating. The peak at 1430 cm^{-1} can be assigned to the asymmetric C-O stretching mode of carboxylate groups covalently bond with ferric or ferrous ions on the surface of the particles. [45] After surface coating, the absorption at 1430 cm^{-1} is enhanced. These observations indicate that PAA coating is achieved by carboxylic groups coordinating with iron atoms in the particles.

To quantify PAA coating, TGA of PAA@USPIOs was performed (Figure S2). Weight loss below 200 ^{o}C can be attributed to the removal of the bound water. [46] PAA coating accounts for

58.26% of total weight (weight loss between 200 °C ~ 900 °C) and the remained solid content (Fe_3O_4) is 36.17%. Considering that the average size of the particle is 4.5 nm, we calculated that there are about 48 PAA molecules (MW 5000) coated on an USPIO.

Zeta potential of PAA@USPIOs was -55 mV and the highly negative charge may arise from free carboxylic groups on the particle surface. [47, 48] To quantify the free carboxylic groups, titration of PAA@USPIOs (0.4 mL) with sodium hydroxide (0.1 M) was performed (Figure S3). The concentration of free carboxylic groups in the sample was 0.16 M. By measuring the iron concentration of the sample (6.28 mg/mL), we determined that the concentration of USPIOs is 8.72 mg/mL and the free carboxylic groups per USPIO are about 2739. Therefore, around 573 carboxylic groups coordinated with surface iron ions considering 48 PAA molecules coated on an USPIO with 69 carboxylic groups per molecule.

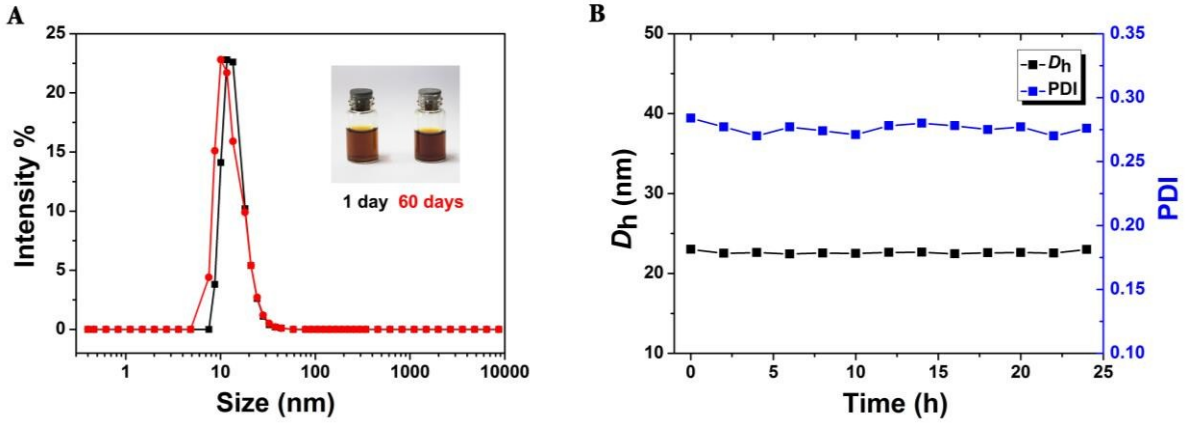

Figure 3 A, Size distribution of PAA@USPIOs in PBS (pH = 7.4) at 25 °C. The size was measured at day1 (black) and day 60 (red) and the particles were suspended in PBS. Insert: photograph of PAA@USPIOs suspension. B, Hydrodynamic diameter of PAA@USPIOs (Dh, black) and PDI (blue) of PAA@USPIOs in 50% (v/v, in PBS) FBS.

Colloidal stability is crucial for biological applications of USPIOs. Next, we evaluated the stability of PAA@USPIOs under physiological conditions by measuring the hydrodynamic diameter of the particles using dynamic light scattering technique (Zetasizer Nano Series Nano-ZS, Malvern Instruments, UK). For this purpose, the particles were spry-dried and autoclave-sterilized, and then suspended in phosphate buffer solution (PBS, pH=7.4) or fetal bovine serum (FBS, 50% in PBS).The hydrodynamic diameter of the particles is 24.4 nm in PBS and does not changed for two months (24 nm) (Figure 3A). After suspended in FBS, the hydrodynamic size decreased a little (22.5 nm), but the particles are stable (Figure 3B). The excellent stability of the particles may arise from the high efficient PAA coating with around 80% of free carboxylic groups on the surface, which could stabilize the particles by both steric hindrance of the polymer and a large electrostatic repulsion effect.

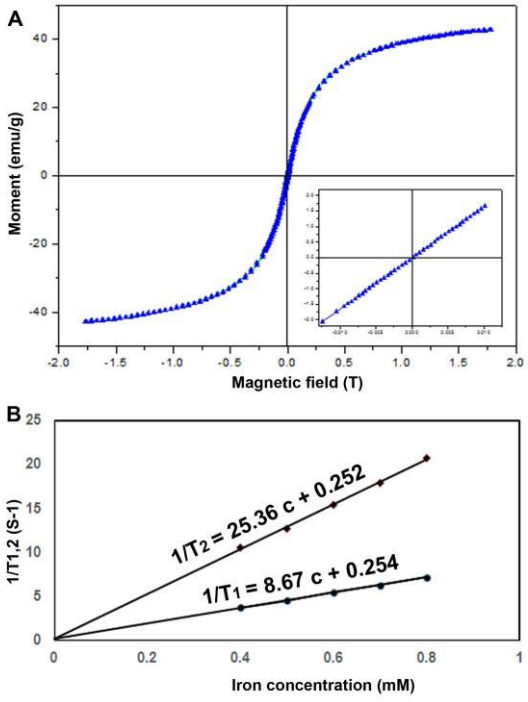

Figure 4 A, Magnetization curve of PAA@USPIOs at room temperature. Insert: magnetization of the particles around zero magnetic field. B, Relaxivities of PAA@USPIOs at 1.41 T.

Superparamagetism is critical for *in vivo* uses of iron oxide nanoparticles. To examine if PAA@USPIOs is superparamagnetic, the susceptibility of the particles as a function of applied magnetic field was evaluated. As shown in Figure 4A, the saturation magnetization of PAA@USPIOs is 42.63 emu g^{-1} and the magnetization is proportional to applied field at low strength, showing no remanence and coercivity (Figure 4A, insert), which indicates that the particles are superparamagnetic at room temperature. [49, 50]

The longitudinal relaxivity (r_1) and the ratio of transverse (r_2) to longitudinal relaxivity (r_2/r_1) are important parameters to estimate the efficiency of USPIOs as T_1 contrast agent. High r_1 and low r_2/r_1 are beneficial for T_1-weighted MRI. [1, 51] Therefore, we determined the r_1 and r_2 relaxivities of PAA@USPIOs by fitting the inverse relaxation times ($1/T_{1,2}$) as functions of the iron concentrations (Figure 4B). The r_1 and r_2 relaxivities of PAA@USPIOs were 8.67 and 25.36 s^{-1} mM^{-1}, respectively, with r_2/r_1 ratio equal to 2.93. The r_1 value is much higher than that of conventional Magnevist (Gd-DTPA, r_1 = 3.6 s^{-1} mM^{-1} at 1.41 T). [52] The r_1 value and r_2/r_1 ratio are also competitive to SHU555C (r_1 = 10.7, r_2 = 38 mM^{-1} s^{-1}, r_2/r_1= 3.6). [53] These results indicate that PAA@USPIOs could be efficient for T_1-weighted MRI. The T_1 effect of PAA@USPIOs may arise from its small size and high colloidal stability. Companying particle size decrease, the magnetic moment of the particles decreases, while surface area with five unpaired electrons in the ferric ion increases, which result in suppression of T_2 effect, but enhancement in T_1 effect. In addition, the colloidal stability of USPIOs is also crucial for its T_1 effect. [32, 54] Aggregation of USPIOs would lead to a dramatic increase in r_2 but an unnoticeable change in r_1, significantly reducing the T_1 effect. [13, 55-57]

Phantom Study The T_1 effect of PAA@USPIOs was first examined by phantom study. For this purpose, PAA@USPIOs was dispersed into water with different concentrations, and T_1- and T_2-weighted MR imaging of the samples were then performed. As shown in Figure 5A, for T_1-weighted MRI images, the MRI signal intensity increased with the increase of particle concentrations. While, for T_2-weighted MRI images, the signal intensity decreased gradually.

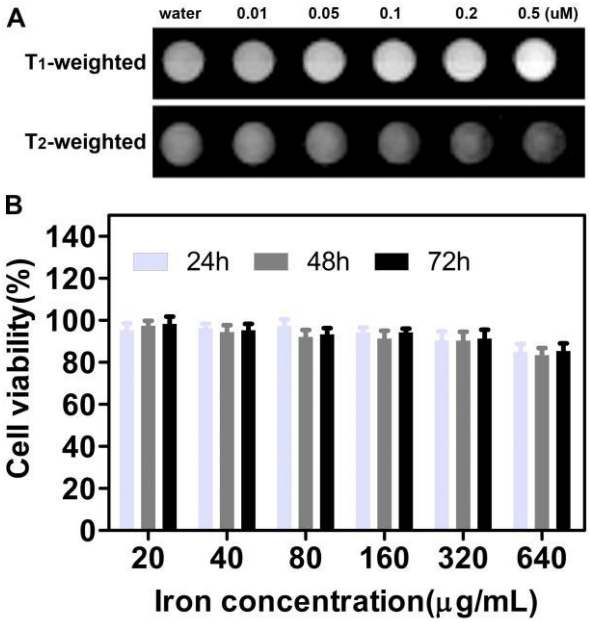

Figure 5 A, T_1 and T_2-weighted MR images of PAA@USPIOs at different concentrations. B, Viability of cells incubated with PAA@USPIOs at different concentrations for different periods of time.

Cytotoxicity of PAA@USPIOs In order to assess the cytotoxicity of PAA@USPIOs, a cell viability assay was evaluated by a typical 3-(4, 5-dimethylthiazol-2-yl)-2, 5-diphenyltetrazolium bromide (MTT) reduction assay using a mouse fibroblast cell line (L929). For this purpose, L929 cells were incubated with PAA@USPIOs at different concentrations (20, 40, 80, 160, 320 and 640 μg/mL in iron) for different periods of time (24, 48 and 72 h). As indicated in Figure 5B, the cell viability was not affected below the dose of 320 μg Fe/mL. Even incubated at the dose of

640 μg Fe/mL for 72 h, there are still more than 90% of cell alive. Consistent with previous reports, [6] our results indicate that PAA@USPIOs are biocompatible and have no obvious toxicity to normal cells.

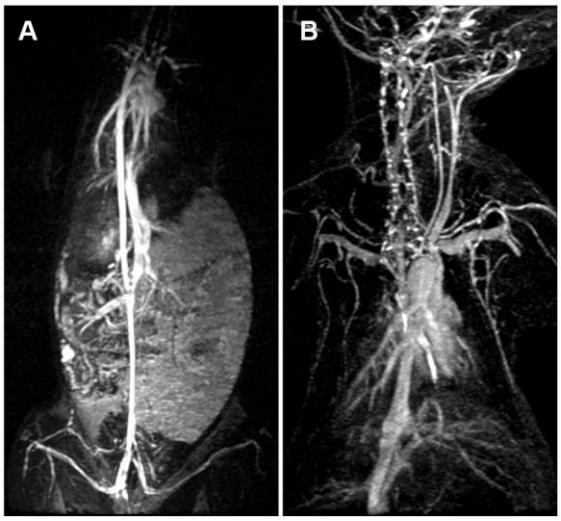

Figure 6 A, B, MRA of rabbit abdomen aorta (A) and head-neck vasculatures (B) after injection of 135 μmol Fe/kg of PAA@USPIOs. Due to the blood pool effect, even small arteries and veins are visible.

Magnetic resonance angiography (MRA) To evaluate T_1 contrast effect of PAA@USPIOs *in vivo* and optimize the dose for blood vessel imaging, MR imaging of rabbit blood vessels with different doses of PAA@USPIOs was conducted. Figure S4 shows T_1-weighted MR images of rabbit abdominal aorta in sagittal orientation at different time periods post PAA@USPIOs injection. Abdominal aorta could be well depicted by all the doses (20, 40, 70, 85, 100, 135 and 200 μmol Fe/kg) investigated during these own optimal imaging windows. However, dose at 135 μmol Fe/kg has the longest imaging window (over 30 min) and demonstrates superior imaging quality. As shown in Figure 6, at this dose, excellent visualization of the abdominal artery and

head-neck vasculatures could be achieved, and even very small vessels such as renal arteries and their ramifications were also depicted with a highly detailed resolution.

First-pass imaging is a technique that acquires three dimensional data sets during the arterial passage of a low-molecular T_1-shortening gadolinium-based contrast medium (e. g. Gd-DTPA) injected in bolus into a peripheral vein. However, due to the rapid extravasation of the contrast medium (10 - 25 s) outside the blood vessels producing a background signal, the spatial resolution of first-pass MRA is limited. To check whether bolus injection of PAA@USPIOs enhances the signal of the abdominal aorta in rabbits in first-pass MRA to a similar extent as a low-molecular contrast medium, first-pass imaging comparing with Gd-DTPA (200 μmol /kg, Magnevist; Schering, Berlin, Germany) was performed. As shown in Figure 7，PAA@USPIOs could depict abdominal aorta with comparable SNR to Gd-DTPA (5.62 *vs* 6.27), but with about two third of its dose (135 μmol Fe/kg).

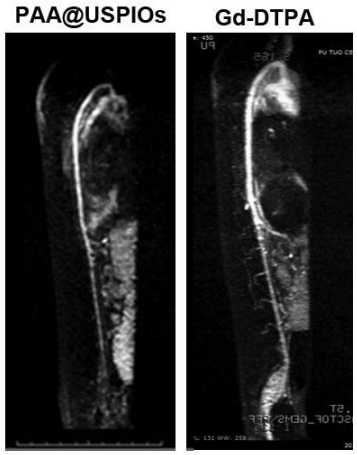

Figure 7 Comparison of PAA@USPIOs to Magevist for the first-pass MRA.

SHU555C (Schering AG, Berlin, Germany) is an iron oxide based MRI contrast agent with a mean core particle size of about 3~5 nm and a mean hydrodynamic diameter of about 21 nm in

an aqueous environment, [58] which has been demonstrated very suitable for both first-pass contrast enhanced MRA comparable to gadolinium-enhanced angiography and high-resolution steady-state angiography pre-clinically. [59] Due to the comparable size of PAA@USPIOs to SHU555C, next, we compared the efficiency of PAA@USPIOs in first-pass and equilibrium MRA with SHU555C. All the contrast agents were injected in bolus with the doses of 135 μmol Fe/kg. Figure 8 shows the MR images of rabbit vascular systems in sagittal orientation at different time points after the particle injection. PAA@USPIOs and SHU555C could depict abdominal aorta in both first-pass and equilibrium imaging.

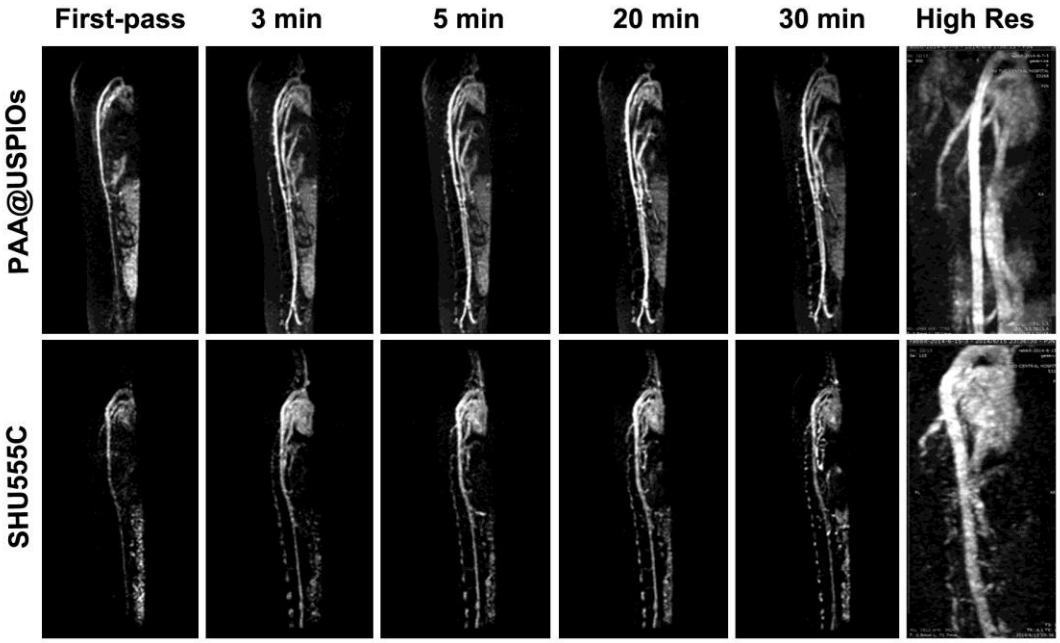

Figure 8 Comparison of PAA@USPIOs to SHU555C for the first-pass and equilibrium MRA.

However, venous vasculatures, even hepatic portal vein, were clearly delineated by PAA@USPIOs, but not by SHU555C. Signal intensity in aortic lumen enhanced by PAA@USPIOs was more pronounced in first-pass (SNR, 35.92 ± 3.11 *vs* 29.01 ± 1.37, $p < 0.01$) and steady-state imaging after the particle injection (SNR, 3min: 30.63 ± 3.42 *vs* 25.30 ± 1.42, p

< 0.01; 5 min: 28.19 ± 2.34 *vs* 21.63 ± 2.23, p < 0.01; 10 min: 25.10 ± 2.39 *vs* 17.60 ± 2.07, p < 0.01; 20 min: 20.93 ± 3.01 *vs* 14.77 ± 2.66, p < 0.01; 30 min: 15.32 ± 1.92 *vs* 10.83 ± 0.39, p < 0.01). In addition, the signal intensity was also more homogenous and much sharper on the vessel edges 30 min post injection.

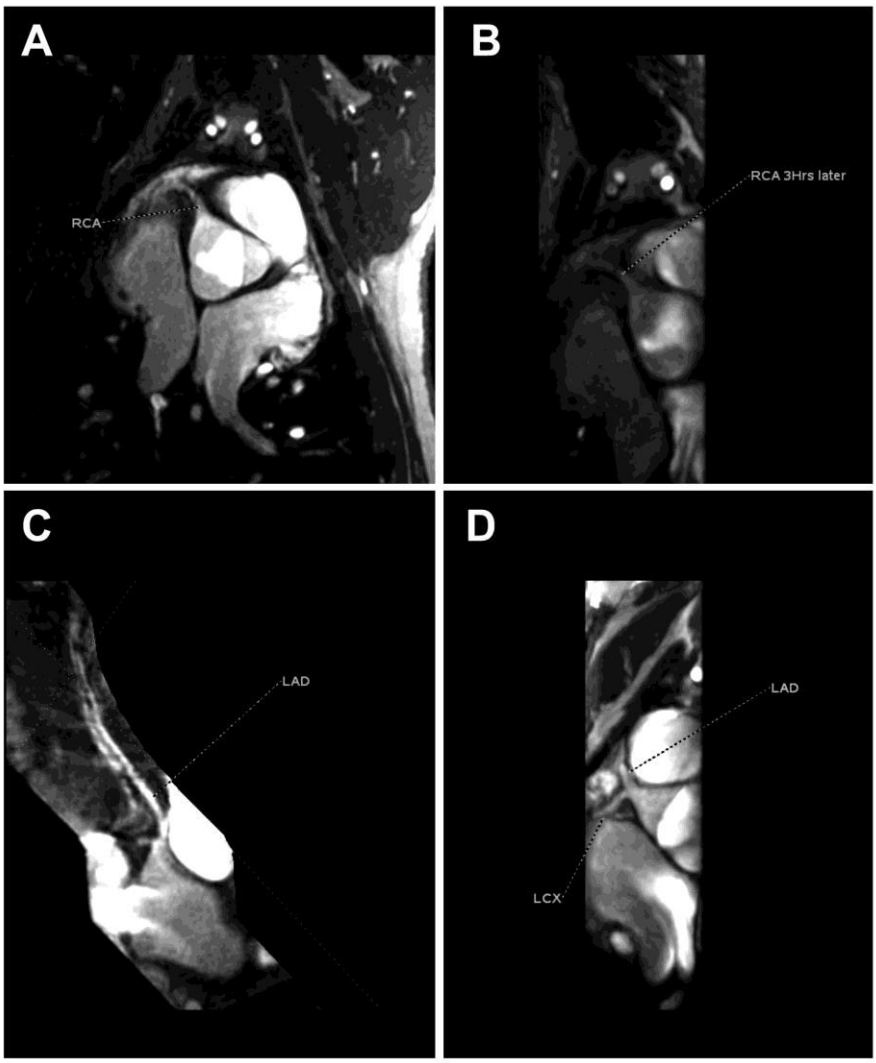

Figure 9 Coronary MRA of pigs. A, B: MRA of the right coronary artery at 15 min (A) and 180 min (B) post PAA@USPIOs injection. C, D: MRA of the left anterior descending branch (LAD) and the left cyclotron (LCX) at 15 min post PAA@USPIOs injection.

Coronary MRA in pigs Due to the small size of coronary artery, coronary MRA is challenging. To further demonstrate the T_1 effect of PAA@USPIOs in vivo, coronary MRA of

pigs was performed. Intravenous injection of PAA@USPIOs at a dosage of 135 μmol Fe/kg produced a pronounced and long-lasting increase in $SNR_{myocardium}$ up to 180 minutes after injection, which resulted in a markedly increased contrast between coronary arteries and myocardium (Figure 9). This effect enables the visualization of large portions of the right coronary arteries (RCA), the left anterior descending branch (LAD) and the left cyclotron (LCX). The $SNR_{myocardium}$ at 15 min post injection was around 9.

Acute single dose toxicity The acute toxicity of PAA@USPIOs was assessed by determination of the LD50 value of mice in 14 h with the modified Spearman-Karber method. [35] For this purpose, five dose levels of PAA@USPIOs ranging from 0.25 to 4 mmol Fe/kg (0.25, 1, 2, 3 and 4 mmol Fe/kg) were examined after single bolus injection with ten animals in each dose group. All the mice survived in the 0.25 and 1 mmol Fe/kg group and no abnormal behaviors were observed. However, with further increase in injection doses, mice presented apnea, twitch, mania or convulsion, indicating that PAA@USPIOs may have the potential side effects on heart, lung or nerve system at these doses. The LD_{50} determined is 2.16 mmol Fe/kg. The dose used in this study (0.135 mmol Fe/kg) for MRA is far below LD50 and no adverse effects to the mice have been observed.

Repeated dose toxicity in mice To determine whether PAA@USPIOs causes the long-term toxicity during its retention in the body, the histological assessment of major organs, hematology analysis and blood biochemical assay were performed. [60, 61] For these purposes, mice were injected with PAA@USPIOs at the doses of 0.73, 1.46 and 2.92 mmol Fe/kg, and the evaluations were performed two days after the end of the treatment period. Figure 10 shows the representative H&E staining images of different tissues. In the treated animals, PAA@USPIOs accumulate mainly in the liver and spleen (brown color) at all the doses investigated, and do not

accumulate in kidney and heart. No notable lesion, inflammation, or other abnormality in these organs associated with the administration of PAA@USPIOs was observed compared to those in the control group. In blood routine examination, white blood cells (WBC), red blood cells (RBC), hemoglobin (HGB), mean corpuscular volume (MCV), mean corpuscular hemoglobin (MCH), mean corpuscular hemoglobin concentration (MCMC), percentage of lymphocyte in white blood cells (LY), percentage of neutrophile granulocyte in white blood cells (NE) and platelet count (PLT) as main parameters were evaluated as the possible toxicity of PAA@USPIOs to mice. The results show that all the parameters mentioned above in the PAA@USPIOs-treated groups

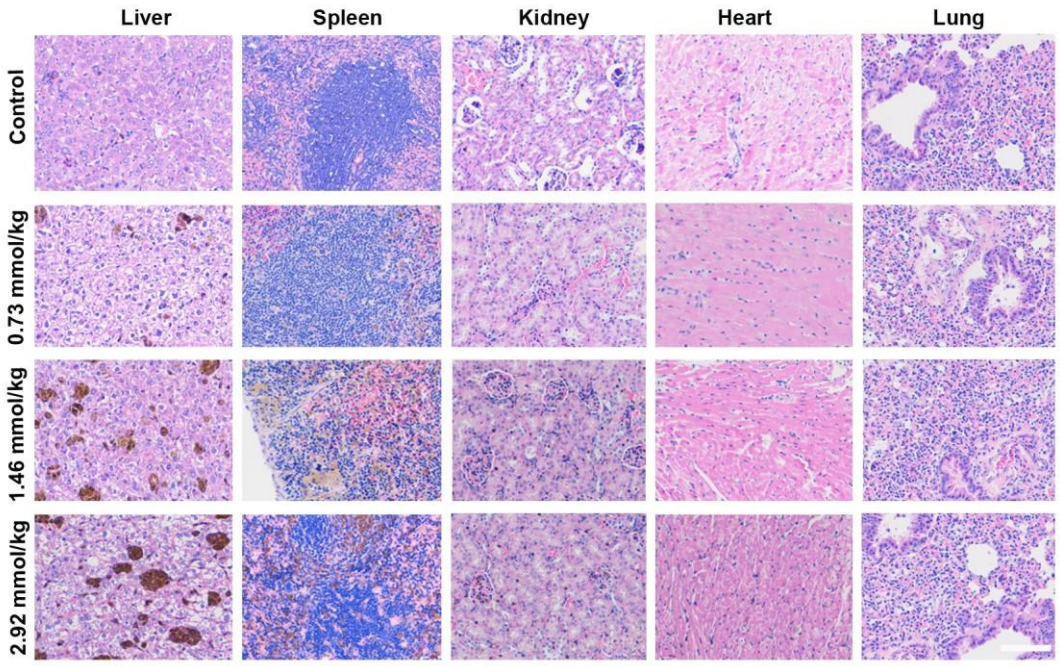

Figure 10 H&E staining of major organs of mice injected with different doses of PAA@USPIOs. Bar: 10 μm.

appear to be normal compared to those in the control group at the doses of 0.73 mmol Fe/kg. When the doses increased to 1.46 and 2.92 mmol/kg, WBC and NE are elevated and other parameters are normal (SI Table 1). In blood chemistry analysis, the liver function markers

including alkaline phosphatase (ALP), aspartate aminotransferase (AST), alanine aminotransferase (ALT) and serum albumin (ALB), kidney function marker urea nitrogen (BUN), as well as albumin/globin ratio, were measured. However, most of the blood biochemical parameters determined above were abnormal (SI Table 2). Considering that high dose was applied for this study, much higher than that used for MRA (0.135 mmol/kg), abnormality of blood biochemical parameters at this dose is not surprising.

4. Conclusions

Microwave-assisted polyol procedure in the presence of poly(acrylic acid) (PAA) is a novel, easy scale-up method for preparation of USPIOs with a yield of 1.5 kg in one batch. The TEM size of the as-prepared USPIOs is around 4.5 nm and the particles are efficiently coated with PAA with around 48 PAA molecules attached on an USPIO, which make the particles highly stable in the physiological conditions. PAA@USPIOs demonstrates good T_1 contrast effect with the r_1 relaxivity of 8.67 s^{-1} mM^{-1} and the r_2/r_1 ratio of 2.93 and superior efficiency in both first-pass and equilibrium MRA. After injected intravenously at the dose of 135 μmol Fe/kg, the head-neck vasculatures and abdominal artery of rabbits and even the coronary artery of pigs could be clearly visualized by T_1-weighted MRI. More significantly, the particles have a good biocompatibility with LD_{50} value of 2.16 mmol Fe/kg for mice. Altogether, PAA@USPIOs prepared by this procedure has great potential for T_1-weighted MRI and for further development for clinical uses.

Acknowledgements

This work was supported by the National Natural Science Foundation of China (81230030, 81571729), the Grants from the State Key Laboratory of Oncogenes and Related Genes (90-15-03), the Med-Engineering Crossing Foundation of SJTU (YG2012MS15), Xinglin scholar training program of Shanghai University of Traditional Chinese Medicine, 315 talent program of Putuo District and Construct Program of the Key Discipline of State Administration of Traditional Chinese Medicine of People's Republic of China.

Notes and references

1. E. Peng, F. Wang and J. M. Xue, *J. Mater. Chem. B*, 2015, **3**, 2241-2276.
2. J. Xie, N. Gu and Y. Zhang, *Advances in Nanotheranostics II: Cancer Theranostic Nanomedicine*, 2016, 39-74.
3. A. Usman, U. Sadat, A. J. Patterson, T. Y. Tang, K. Varty, J. R. Boyle, M. P. Armon, P. D. Hayes, M. J. Graves and J. H. Gillard, *Nanomedicine (Lond)*, 2015, **10**, 3077-3087.
4. N. Schleich, F. Danhier and V. Préat, *Journal of Controlled Release*, 2015, **198**, 35-54.
5. A. G. Roca, S. Veintemillas-Verdaguer, M. Port, C. Robic, C. J. Serna and M. P. Morales, *J. Phys. Chem. B*, 2009, **113**, 7033-7039.
6. G. Wang, X. Zhang, A. Skallberg, Y. Liu, Z. Hu, X. Mei and K. Uvdal, *Nanoscale*, 2014, **6**, 2953–2963.
7. G. Kandasamy and D. Maity, *International Journal of Pharmaceutics*, 2015, **496**, 191-218.
8. Z. Zhou, C. Wu, H. Liu, X. Zhu, Z. Zhao, Wang, L., Y. Xu, H. Ai and J. Gao, *ACS Nano*, 2015, **9**, 3012–3022.

9. T. Borase, T. Ninjbadgar, A. Kapetanakis, S. Roche, R. O'Connor, C. Kerskens, A. Heise and D. F. Brougham, *Angew. Chem. Int. Ed.*, 2013, **52**, 3164 -3167.

10. L. Sandiford, A. Phinikaridou, A. Protti, L. K. Meszaros, X. Cui, Y. Yan, G. Frodsham, P. A. Williamson, N. Gaddum, R. M. Botnar, P. J. Blower, M. A. Green and R. T. M. Rosales, *ACS Nano*, 2013, **7**, 500–512.

11. B. H. Kim, N. Lee, H. Kim, K. An, Y. I. Park, Y. Choi, K. Shin, Y. Lee, S. G. Kwon, H. B. Na, J.-G. Park, T.-Y. Ahn, Y.-W. Kim, W. K. Moon, S. H. Choi and T. Hyeon, *J. Am. Chem. Soc.*, 2011, **133**, 12624-12631.

12. J. Bremerich, D. Bilecen and P. Reimer, *Eur Radiol* 2007, **17**, 3017-3024.

13. U. I. Tromsdorf, O. T. Bruns, S. C. Salmen, U. Beisiegel and H. Weller, *Nano Letters*, 2009, **9**, 4434-4440.

14. S. Laurent, D. Forge, M. Port, A. Roch, C. Robic, L. Vander and R. Muller, *Chem. Rev.*, 2008, **108**, 2064-2110.

15. Y. Hou, J. Yu and X. Chu, *Advances in Nanotheranostics II: Cancer Theranostic Nanomedicine*, 2016, 3-38.

16. V. Weissig and D. Guzman-Villanueva, *International Journal of Nanomedicine*, 2015, **10**, 1245-1257.

17. E. Kim, K. Lee, Y.-M. Huh and S. Haam, *J. Mater. Chem. B*, 2013, **1**, 729-739.

18. B. Tombach, P. Reimer, M. Mahler, W. Ebert, C. Pering and W. Heindel, *Acad Radiol* 2002, **9**, S425-S427.

19. S. H. Sun and H. Zeng, *J. Am. Chem. Soc.*, 2002, **124**, 8204-8205.

20. J. Park, K. An, Y. Hwang, J.-G. Park, H.-J. Noh, J.-Y. Kim, J.-H. Park, N.-M. Hwang and T. Hyeon, *Nat. Mater.*, 2004, **3**, 891-895.

21. J. Kim, J. E. Lee, S. H. Lee, J. H. Yu, J. H. Lee, T. G. Park and T. Hyeon, *AdV. Mater.* , 2008, **20**, 478-483.

22. Z. Zhou, X. Zhu, D. Wu, Q. Chen, D. Huang, C. Sun, J. Xin, K. Ni and J. Gao, *Chem. Mater.*, 2015, **27**, 3505-3515.

23. Y. Li, F. Ma, X. Su, L. Shi, B. Pan, Z. Sun and Y. Hou, *Ind. Eng. Chem. Res.*, 2014, **53**, 6718-6722.

24. D. Ling and T. Hyeon, *Small* 2013, **9**, 1450-1466.

25. D. Ling, N. Lee and T. Hyeon, *Acc. Chem. Res.*, 2015, **48**, 1276-1285.

26. B. I. Kharisov, H. V. R. Dias, O. V. Kharissova, A. Vazquez, Y. Pena and I. Gomez, *RSC Advances*, 2014, **4**, 45354-45381.

27. B. I. Kharisov, H. V. R. Dias, O. V. Kharissova, A. V´azquez, Y. Pe˜na and I. G´omez, *RSC Adv.*, 2014, **4**, 45354–45381.

28. J. Liu, Z. Sun, Y. Deng, Y. Zou, C. Li, X. Guo, L. Xiong, Y. Gao, F. Li and D. Zhao, *Angew. Chem., Int. Ed.*, 2009, **48**, 5875-5879.

29. X. Jia, D. Chen, X. Jiao and S. Zhai, *Chem. Commun.*, 2009, 968-970.

30. N. Miguel-Sancho, O. Bomat´ı-Miguel, G. Colom, J. P. Salvador, M. P. Marco and J. Santamaria, *Chem. Mater.*, 2011, **23**, 2795-2802.

31. F. Hu and Y. S. Zhao, *Nanoscale*, 2012, **4**, 6235–6243.

32. F. Hu, Q. Jia, Y. Li and M. Gao, *Nanotechnology*, 2011, **22**, 245604.

33. S. Xue, C. Zhang, Y. Yang, L. Zhang, D. Cheng, J. Zhang, H. Shi and Y. Zhang, *J. Biomed. Nanotechnol.*, 2015, **11**, 1027-1037.

34. M. Li, H. Gu and C. Zhang, *Nanoscale Research Letters* 2012, **7**, 204.

35. M. A. Hamilton, R. C. Russo and R. V. Thurston, *Environ. Sci. Technol.*, 1977, **11**, 714–719.

36. Q. Wang, M. Shen, T. Zhao, Y. Xu, J. Lin, Y. Duan and H. Gu, *Scientific Reports*, 2015, **5** 7774.

37. A. J. Cole, A. E. David, J. Wang, C. J. Galban and V. C. Yang, *Biomaterials*, 2011, **32**, 6291-6301.

38. L. Xiao, J. Li, D. F. Brougham, E. K. Fox, N. Feliu, A. Bushmelev, A. Schmidt, N. Mertens, F. Kiessling, M. Valldor, B. Fadeel and S. Mathur, *ACS Nano*, 2011, **5**, 6315-6324.

39. L.-H. Shen, J.-F. Bao, D. Wang, Y.-X. Wang, Z.-W. Chen, L. Ren, X. Zhou, X.-B. Ke, M. Chen and A.-Q. Yang, *Nanoscale*, 2011, **5**, 2133 – 2141.

40. S. Xuan, Y. X. J. Wang, J. C. Yu and K. Cham-Fai Leung, *Chem. Mater.*, 2009, **21**, 5079-5087.

41. Y. J. Zhu and F. Chen, *Chem. Rev.*, 2014, **114**, 6462-6555.

42. A. M. Schwenke, S. Hoeppener and U. S. Schubert, *AdV. Mater.*, 2015, **27**, 4113-4141

43. M. Baghbanzadeh, L. Carbone, P. D. Cozzoli and C. O. Kappe, *Angew. Chem., Int. Ed.*, 2011, **50**, 11312-11359.

44. K. Y. Bae, Y. B. Kim, Y. Lee, J. Y. Hwang, H. W. Park and T. G. Park, *Bioconjugate Chem.* , 2010, **21**, 505-512.

45. D. Lee, R. Condrate and J. Reed, *Journal of Materials Science*, 1996, **31**, 471-478.

46. S. Chen, G. Wu, Y. Liu and D. Long, *Macromolecules*, 2006, **39**, 330-334.

47. J. W. Zhang, M. S. Azam, C. Shi, J. Huang, B. Bin, Q. X. Liu and H. B. Zeng, *RSC Advances,* 2015, **5**, 32272-32282.

48. C.-S. Chiang, Y.-H. Tseng and B.-J. Liao, *Adv. Health. Mater.*, 2015, **4**, 1066-1075

49. Y. Liu, Y. Wang, S. Zhou, S. Lou, L. Yuan, T. Gao, X. Wu, X. Shi and K. Wang, *ACS Appl. Mater. Interfaces*, 2012, **4**, 4913-4920.

50. M. E. Zilm, M. Staruch, M. Jain and M. Wei, *J. Mater. Chem. B* 2014, **2**, 7176-7185.

51. M. Zhang, Y. Cao, L. Wang, Y. Ma, X. Tu and Z. Zhang, *ACS Appl. Mater. Interfaces* 2015, **7**, 4650-4658.

52. S.-B. Yu and A. D. Watson, *Chem. Rev.*, 1999, **99**, 2353.

53. C. Corot, P. Robert, J.-M. Idée and M. Port, *Advanced Drug Delivery Reviews*, 2006, **58**, 1471-1504.

54. A. Roch, R. N. Muller and P. Gillis, *J. Chem. Phys.*, 1999, **110**, 5403.

55. K. C. Barick, M. Aslam, Y.-P. Lin, D. Bahadur, P. V. Prasad and V. P. Dravid, *J. Mater. Chem.*, 2009, **19**, 7023-7029.

56. Y. Wang, F. Xu, C. Zhang, D. Lei, Y. Tang, H. Xu, Z. Zhang, H. Lu, X. Du and G.-Y. Yang, *Nanomedicine: NBM*, 2011, **7**, 1009-1019.

57. C. Zhang, X. Xie, S. Liang, M. Li, Y. Liu and H. Gu, *Nanomedicine: NBM*, 2012, **8**, 996–1006.

58. R. Lawaczeck, H. Bauer, T. Frenzel, M. Hasegawa, Y. Ito, K. Kito, N. Miwa, H. Tsutsui, H. Vogler and H. J. Weinmann, *Acta Radiol*, 1997, **38(4 Pt 1)**, 584-597.

59. B. Tombach, P. Reimer, C. Bremer, T. Allkemper, M. Engelhardt, M. Mahler, W. Ebert and W. Heindel, *NMR Biomed*, 2004, **17**, 500-506.

60. K. Yang, G. Yang, L. Chen, L. Cheng, L. Wang, C. Ge and Z. Liu, *Biomaterials*, 2015, **38**, 1-9.

61. K. Dong, Z. Liu, J. Liu, S. Huang, Z. Li, Q. Yuan, J. Ren and X. Qu, *Nanoscale* 2014, **6**, 2211-2217.

TOC abstract

Ultra-large-scale production of ultrasmall superparamagnetic iron oxide nanoparticles for magnetic resonance angiography